Biochimica et Biophysica Acta 1842 (2014) 1010–1016

Contents lists available at ScienceDirect

Biochimica et Biophysica Acta

journal homepage: www.elsevier.com/locate/bbadis

Alternating Hemiplegia of Childhood mutations have a differential effect on Na^+,K^+-ATPase activity and ouabain binding

Karl M. Weigand [a], Muriël Messchaert [a], Herman G.P. Swarts [b], Frans G.M. Russel [a], Jan B. Koenderink [a,*]

[a] Department of Pharmacology and Toxicology 149, Radboud University Medical Centre, P.O. Box 9101, 6500 HB Nijmegen, The Netherlands
[b] Department of Biochemistry 286, Radboud University Medical Centre, P.O. Box 9101, 6500 HB Nijmegen, The Netherlands

ARTICLE INFO

Article history:
Received 27 November 2013
Received in revised form 26 February 2014
Accepted 2 March 2014
Available online 12 March 2014

Keywords:
AHC
Alpha 3
Alternating Hemiplegia of Childhood
ATP1A3
Na^+,K^+-ATPase

ABSTRACT

De novo mutations in *ATP1A3*, the gene encoding the α3-subunit of Na^+,K^+-ATPase, are associated with the neurodevelopmental disorder Alternating Hemiplegia of Childhood (AHC). The aim of this study was to determine the functional consequences of six *ATP1A3* mutations (S137Y, D220N, I274N, D801N, E815K, and G947R) associated with AHC. Wild type and mutant Na^+,K^+-ATPases were expressed in Sf9 insect cells using the baculovirus expression system. Ouabain binding, ATPase activity, and phosphorylation were absent in mutants I274N, E815K and G947R. Mutants S137Y and D801N were able to bind ouabain, although these mutants lacked ATPase activity, phosphorylation, and the K^+/ouabain antagonism indicative of modifications in the cation binding site. Mutant D220N showed similar ouabain binding, ATPase activity, and phosphorylation to wild type Na^+,K^+-ATPase. Functional impairment of Na^+,K^+-ATPase in mutants S137Y, I274N, D801N, E815K, and G947R might explain why patients having these mutations suffer from AHC. Moreover, mutant D801N is able to bind ouabain, whereas mutant E815K shows a complete loss of function, possibly explaining the different phenotypes for these mutations.

1. Introduction

Alternating Hemiplegia of Childhood (AHC) is a rare, severe neurodevelopmental disorder, reported for the first time in 1971 by Verret and Steele [1]. The incidence of AHC has been estimated at 1 in 1,000,000 births, with disease usually ensuing within the first six months [2]. AHC is characterized by episodes of hemiplegia on alternating sides of the body [3], which can last from a few minutes up to several days. Other symptoms that can occur during AHC episodes include pallor, abnormal eye movements, movement disorders, dystonia and severe cognitive impairment [4]. Patient studies have reported different provoking factors: water exposure, extreme temperatures, physical activity, bright light, and stress [5]. Falling asleep leads to disappearance of all symptoms, although they may return after waking up. The exact mechanism of disease is unknown, although treatment with Flunarizine (a Ca^{2+} influx inhibitor specific for vascular smooth muscle and neurons) has been reported to reduce symptoms [6,7]. However, the effectiveness and long-term effects of this treatment are unknown [5].

AHC was recently linked to de novo mutations in *ATP1A3*, the gene encoding the Na^+,K^+-ATPase α3 subunit [8,9]. Most mutations are located in or near the ten transmembrane domains of Na^+,K^+-ATPase. Interestingly, two mutations (D801N and E815K) found in 66% of the AHC patients show differences with regard to disease severity, where E815K has been associated with a more severe phenotype [10]. Previously, *ATP1A3* mutations were identified in patients suffering from Rapid-Onset Dystonia Parkinsonism (RDP) [11]. Until now, there has been only one mutation that is reported in AHC and RDP cases (D923N), indicating minor overlap between both diseases [12–14].

Na^+,K^+-ATPase plays a major role in maintaining the electrochemical gradient across the plasma membrane. The α-subunit is the catalytic component of this transport protein, which together with the β-subunit forms a functional transporter enzyme, in some tissues accompanied by a third or gamma subunit. In humans, four different isoforms of the α-subunit exist. Three of these isoforms are expressed in the human brain: α1 in multiple cell types due to its ubiquitous expression, including neurons and glial cells, α2 predominantly in astrocytes, and α3 in peripheral and central nervous system neurons [15,16]. When catalytically active, Na^+,K^+-ATPase transports three sodium ions out of the cell and two potassium ions into the cell, a process fueled by hydrolysis of one molecule ATP [15]. During this catalytic cycle, Na^+,K^+-ATPase is present in the E_1 or the E_2 conformation, depending on the association of either Na^+ or K^+ to the ion binding sites (Fig. 1A). The presence of both ATP and Na^+ is necessary for the phosphorylation of the protein in the E_1 state, which leads to a conformational change into

* Corresponding author at: Department of Pharmacology and Toxicology, Radboud University Medical Centre, P.O. Box 9101, 6500 HB Nijmegen, The Netherlands. Tel.: +31 24 36 13654; fax: +31 24 36 14214.
E-mail addresses: Karl.Weigand@radboudumc.nl (K.M. Weigand), Muriel.Messchaert@radboudumc.nl (M. Messchaert), H.Swarts@ncmls.ru.nl (H.G.P. Swarts), Frans.Russel@radboudumc.nl (F.G.M. Russel), Jan.Koenderink@radboudumc.nl (J.B. Koenderink).

http://dx.doi.org/10.1016/j.bbadis.2014.03.002
0925-4439/

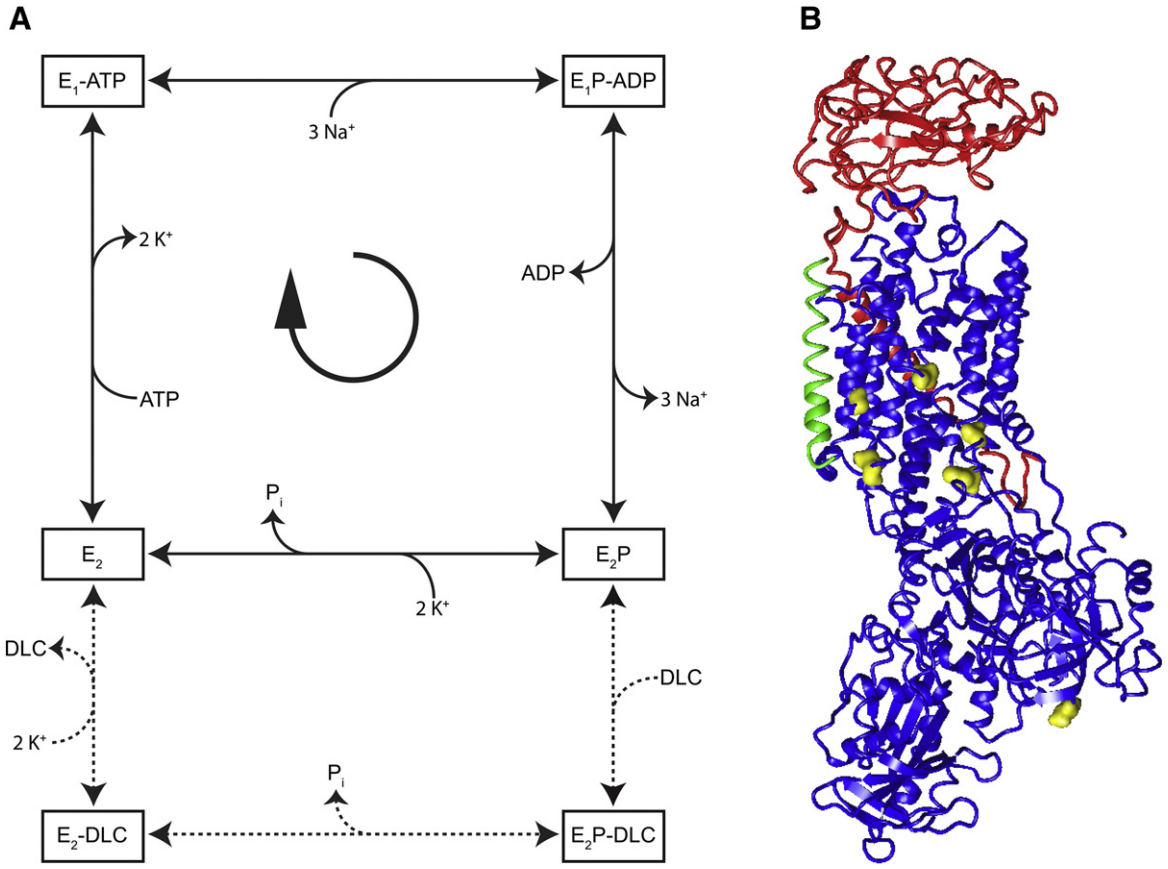

Fig. 1. (A) Albert-Post scheme of the reaction cycle of Na^+,K^+-ATPase. Transport of Na^+ and K^+ across the cell membrane is accomplished by a series of conformational changes of the Na^+,K^+-ATPase based on binding of either Na^+ or K^+, leading to phosphorylation or dephosphorylation, changing the affinity of the enzyme for its ligands. During each reaction cycle, three Na^+ ions are transported out of the cell, in return transporting two K^+ ions into the cell. This process requires the hydrolysis of ATP, to drive the transition into the high energy E_1P and E_2P states. Binding of DLCs, well-known inhibitors of Na^+,K^+-ATPase function, is only possible in the E_2P or E_2 state. (B) Crystal structure of the Na^+,K^+-ATPase heteromer in the E_2 state (PDB: 3KDP) [32], with the location of the six mutations studied here highlighted by spheres. Note how five mutations are located in or near transmembrane regions, whereas mutant D220N is located in the large cytosolic loop between transmembrane domains two and three. The six residues are conserved between the alpha 1 and alpha 3 isoforms, making the alpha 1 crystal structure suitable for representation. Blue is alpha subunit, red is beta subunit, green is gamma subunit, and yellow is used to highlight the mutations studied here. Figure was created using YASARA software.

the Na^+-bound phosphorylated conformation (E_1P–ADP). During transition to the E_2P state, Na^+ is released out of the cell, followed by binding of K^+, which initiates dephosphorylation of the protein and transition into the K^+-bound E_2 state [17]. Binding of ATP drives the protein back into the E_1 state, completing the catalytic cycle.

The effect of *ATP1A3* mutations on protein functionality is hardly studied. Moreover, whether different phenotypes can be linked to specific mutations is not known. In this study, we determined the functional consequences of six de novo *ATP1A3* mutations (S137Y, D220N, I274N, D801N, E815K, and G947R, see Fig. 1B) in order to relate protein functionality to AHC phenotypes.

2. Materials and methods

2.1. The Gateway system

The desired mutations were obtained by first performing two PCRs (A and B) on human Na^+,K^+-ATPase alpha 3 wild type cDNA using either a 5′ or 3′ primer in combination with a primer containing the desired mutation, resulting in two different fragments that were subsequently combined for a final PCR (C) using only the 5′ and 3′ primers, allowing annealing of the two fragments (A and B) containing the desired mutation. Next, the obtained mutant Na^+,K^+-ATPase α3 was cloned into an entry vector using BP Clonase II enzyme according to the manufacturer's instructions (Invitrogen). After a successful transformation of entry clones into DH5α cells and overnight selection, colonies were grown overnight in liquid medium and subsequently isolated using the GenElute™ mini-prep isolation kit (Sigma-Aldrich). Following a restriction analysis, full length sequencing of the different constructs was performed to check for successful mutagenesis. Subsequently, the entry clones were combined with an empty destination vector already containing the β1 gene (*ATP1B1*) using LR Clonase II (Invitrogen), resulting in an expression clone containing the desired mutation. As a negative control, an expression clone containing YFP in combination with the β1 subunit was used for mock transfection.

2.2. Generation of recombinant viruses

The expression clones, generated using the Gateway system, were transformed to competent DH10Bac *Escherichia coli* cells (Life Technologies, Breda, The Netherlands) harboring the baculovirus genome (bacmid) and a transposition helper plasmid. Upon transposition between the Tn7 sites present in both the bacmid and the expression clone, recombinant bacmids were selected and isolated [18]. Subsequently, the obtained bacmids were transfected to Sf9 insect cells using Cellfectin reagent (Life Technologies, Breda, The Netherlands). After a 6-day period, recombinant baculoviruses were harvested and used to infect fresh Sf9 cells at a multiplicity of infection of 0.1. After another 6 days of culture of infected Sf9 cells, amplified baculoviruses were harvested [19].

2.3. Protein production

Sf9 cells grown at 27 °C in T175 and later in 500 mL shaking flasks in Xpress medium (Sigma, Bornem, Belgium) were infected at a density of $1.5 \cdot 10^6$ cells·mL^{-1} in the presence of 1% (v/v) ethanol, as described before [20]. After three days of infection, cells were harvested by centrifugation at 2000 ×*g* for 5 min. Then, the pelleted cells were resuspended at 0 °C in a 250 mM saccharose, 2.0 mM EDTA and 20 mM HEPES/Tris at pH 7.0 buffer. Sonication was performed for 30 s at 80 W prior to centrifugation at 10,000 ×*g* at 4 °C for 30 min, followed by centrifugation of the resulting supernatant at 100,000 ×*g* at 4 °C for 1 h. The pelleted membranes were resuspended in the buffer mentioned above, homogenized, and stored at −20 °C before use in biochemical studies.

2.4. Western blotting

Approximately 20 μg of membranes were treated with SDS-PAGE solubilization buffer overnight at room temperature before loading on a 10% polyacrylamide gel, as described previously [21]. After separation, the proteins were transferred to a polyvinylidene fluoride membrane and subsequently blocked in 5% Elk in TBS-T. Then, α- and β-subunits were detected using either the G36 (anti-α) or the C385-M77 (anti-β) antibody [20,21].

2.5. ATPase activity studies

To determine the ATPase activity in Na^+ or K^+ affinity studies, 20 μL of membranes was incubated in a final volume of 100 μL containing 50 mM Tris–Ac at pH 7.0, 0.1 mM EGTA, 1.25 mM $MgCl_2$, 1.0 mM Tris-N_3, 100 μM of radiolabeled ATP, and 50 mM NaCl or 5.0 mM KCl and increasing concentrations of either KCl or NaCl. After incubation of the samples for 30 min at 37 °C, the reaction was stopped by the addition of 500 μL of 10% (w/v) charcoal in 6% (v/v) trichloroacetic acid and after 10 min at 0 °C the mixture was centrifuged for 30 s. Subsequently, 150 μL of the clear supernatant was mixed with 4 mL OptiFluor before analysis using a liquid scintillation counter to determine the amount of inorganic phosphate (P_i) formed, a measure for ATPase activity [22]. The Na^+,K^+-ATPase specific activity was determined by subtracting the amount of P_i formed in the presence of 1.0 mM ouabain. Maximum ATPase values were determined by measuring the activity in the presence of 50 mM NaCl, 5.0 mM KCl, 1.25 mM $MgCl_2$ and 0.1 mM ATP at pH 7.0.

2.6. Phosphorylation assay

Sf9 membranes were incubated in 60 μL medium, containing 50 mM Tris–acetic acid (pH 7.0), 1.25 mM $MgCl_2$, 100 mM NaCl and in the presence or absence of 10 mM KCl. After 30 min preincubation, 10 μL of 0.6 μM [γ-^{32}P]ATP was added and incubated for 10 s at 0 °C. The reaction was stopped by adding 5% TCA and (phosphorylated) protein was collected by filtration through a 0.8 μm membrane filter. After repeated washing with ice-cold water the filters were added to 4 mL OptiFluor and analyzed by liquid scintillation analysis [22]. Phosphorylation was calculated by subtracting the amount of phosphate detected (phosphorylated protein) in the presence of KCl from the amount obtained in the absence of KCl.

2.7. Ouabain binding experiments

Ouabain binding was determined by incubation of approximately 150–200 μg of membranes in the presence of 20 mM histidine, 5.0 mM $MgCl_2$, 5.0 mM H_3PO_4 at pH 7.0, (varying concentrations of KCl) and 25 nM of radiolabeled ouabain (Perkin-Elmer, Waltham, MA, USA) in a final volume of 60 μL at room temperature for 2 h. After incubation for 15 min on ice, the amount of bound ouabain was determined by washing the samples through a 0.8 μm ME27 filter using H_2O, retaining the enzyme-bound ouabain. The radioactivity retained on the filters was determined in a liquid scintillation counter after the addition of 4 mL OptiFluor (Canberra Packard, Tilburg, The Netherlands) [23].

2.8. Data analysis

All data were analyzed using GraphPad Prism 5.02. Statistical analysis (ANOVA, with Dunnett's post test comparing to mock values, $n \geq 3$ for all experiments and $\alpha = 0.05$) was performed to test for differences in maximum ouabain binding, apparent ouabain affinity, apparent Na^+ and K^+ affinities, maximum phosphorylation levels and maximum ATPase activity levels compared to mock. The $Na^+_{0.5}$ and $K^+_{0.5}$ values were calculated via the Hill equation using the averaged data and SEM values. The Hill coefficient obtained for wild type Na^+,K^+-ATPase was used also for the calculation of the half-maximum Na^+ and K^+ concentrations of mutants.

2.9. Analysis of crystal structures

Three different crystal structures representing α1β1 Na^+,K^+-ATPase in the E_1P–ADP (4HQJ [24]), E_2P–ouabain (4HYT [25]), and $E_2 \cdot 2K^+ \cdot P_i$ (2ZXE [26]) conformations were used to identify possible interactions involving the mutations characterized in the present study. YASARA software (www.YASARA.org) was used to visualize these crystal structures and identify hydrogen (H−) bond interaction networks.

3. Results

3.1. Analysis of expression

Six single mutations associated with AHC (S137Y, D220N, I274N, D801N, E815K, and G947R, see Fig. 1B) were introduced in the α3 subunit of Na^+,K^+-ATPase. Wild type and mutant Na^+,K^+-ATPases were expressed in Sf9 insect cells using the baculovirus expression system. The membrane fractions of these Sf9 cells were isolated and used for biochemical characterization. Similar expression levels for wild type and mutant enzymes were detected by Western blot analysis using antibodies against the α- and β-subunits (Fig. 2).

3.2. Mutant D220N is catalytically active

The Na^+,K^+-ATPase activity of both wild type and mutants was determined in the presence of 100 μM ATP, 5.0 mM KCl and 50 mM NaCl. Five mutants did not show ATPase activity different from mock (Fig. 3). Significantly higher ATPase activities were observed for wild type enzyme and mutant D220N ($p < 0.05$). The activities of wild type enzyme (1.2 ± 0.1 μmol P_i mg^{-1} h^{-1}) and mutant D220N (0.98 ± 0.05 μmol P_i mg^{-1} h^{-1}) were not significantly different. The absence of ATPase activity for the other mutants indicated that these mutations result in a catalytically inactive enzyme.

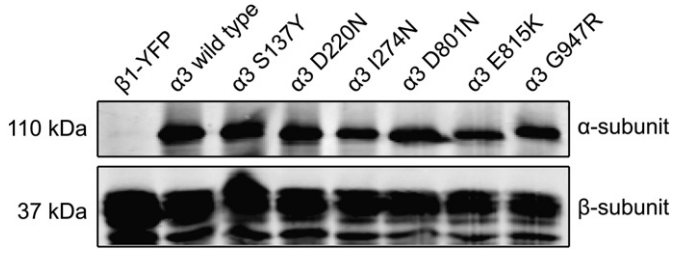

Fig. 2. Western blot of Na^+,K^+-ATPase α- and β-subunits for six different Sf9 membrane preparations. Membranes (20 μg) were run on a 10% SDS-PAGE gel and transferred to a PVDF membrane. The presence of α- and β-subunits was detected using antibodies C356-M09 and C385-M77, respectively [20,21].

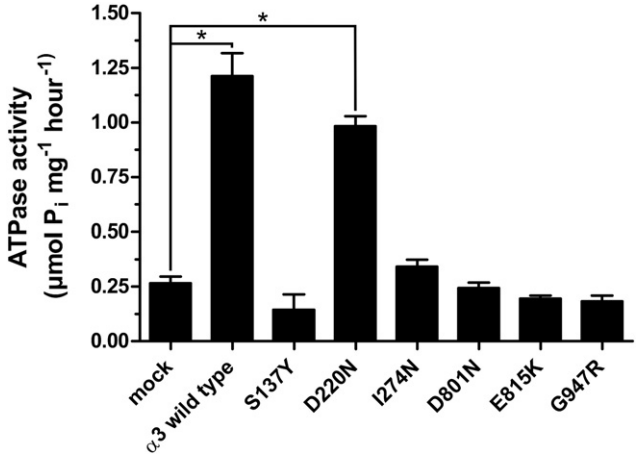

Fig. 3. ATPase activity of mutant and wild type Na^+,K^+-ATPase. Enzymes were incubated at 37 °C in the presence of 1.3 mM $MgCl_2$, 0.1 mM EGTA, 2.0 mM Tris-N_3, 50 mM Tris–acetic acid (pH 7.0), 100 μM radiolabeled ATP, 5.0 mM KCl and 50 mM NaCl for 30 min. Na^+,K^+-ATPase activity was corrected for background by subtracting mock values. Values are presented as mean ± SEM with N ≥ 3. *p < 0.05 versus mock, ANOVA with Dunnett's post test.

3.3. Na^+, K^+, and ATP affinities for mutant D220N and wild type enzyme are similar

Next, we determined the effect of Na^+, K^+ and ATP on the ATPase activity. Since mutant D220N was the only protein that showed ATPase activity, these experiments were performed only for this mutant. The Na^+ affinity was determined by measuring ATPase activity at increasing concentrations of NaCl in the presence of 0.1 mM ATP and 5.0 mM KCl. ATPase activity increased with increasing Na^+ concentration (Fig. 4A), and no significant differences in apparent Na^+ affinity were observed between wild type and the mutant D220N ($K_{0.5}$ of 11 ± 1 mM and 12 ± 1 mM, respectively).

The K^+ affinity was determined by measuring ATPase activity at increasing concentrations of KCl in the presence of 0.1 mM ATP and 50 mM NaCl. As shown in Fig. 4B, there were no significant differences in apparent K^+ affinity between wild type ($K_{0.5}$ = 0.62 ± 0.1 mM) and mutant D220N ($K_{0.5}$ = 0.56 ± 0.1 mM).

The ATP affinity was determined by measuring ATPase activity at increasing ATP concentrations in the presence of 50 mM NaCl and 5.0 mM KCl. Fig. 4C shows no differences in apparent ATP affinity ($K_{0.5}$ of 55 ± 19 μM (wild type) and 86 ± 27 μM (D220N)).

3.4. Phosphorylation capacity

One of the features of the Na^+,K^+-ATPase reaction cycle is phosphorylation of the protein, forming an acid-stable intermediate. Both Na^+ and ATP are necessary for the conformational change of the protein from the E_2 state to the phosphorylated E_2P state. In the absence of K^+ and high levels of Na^+, the enzyme will accumulate in this conformation (Fig. 1A). The phosphorylation capacity of all mutants was determined by measuring the amount of phosphoenzyme (E–P) in the presence of 100 mM NaCl and 0.1 μM ATP, background-corrected for the amount of E–P present when 10 mM KCl was added (allowing dephosphorylation to take place as well). Phosphorylation of mutants S137Y, I274N, D801N, E815K, and G947R was absent (Fig. 5). Mutant D220N showed a phosphorylation level of 1.8 pmol E–P mg^{-1}, similar to wild type enzyme (1.8 pmol E–P mg^{-1}).

3.5. Mutants S137Y, D220N and D801N bind ouabain

The conformational change from E_2 to E_2P–ouabain via E_2P (backdoor phosphorylation) could be determined in the presence of 5 mM P_i and increasing concentrations of [^{3}H]-ouabain. Ouabain binding was observed for wild type Na^+,K^+-ATPase and three mutants: S137Y, D220N, and D801N (Fig. 6A). The other three mutants (I274N, E815K and G947R) showed no ouabain binding. Mutant D801N showed an increase in maximum ouabain binding compared to wild type enzyme (6.6 pmol mg^{-1} versus 1.5 pmol mg^{-1}). Mutant S137Y showed a decreased EO_{max} (1.0 pmol mg^{-1}), whereas mutant D220N exhibited ouabain binding capacity equal to wild type enzyme (1.5 pmol mg^{-1}). Calculated ouabain affinities (K_d) of mutants and wild type enzyme were not significantly different.

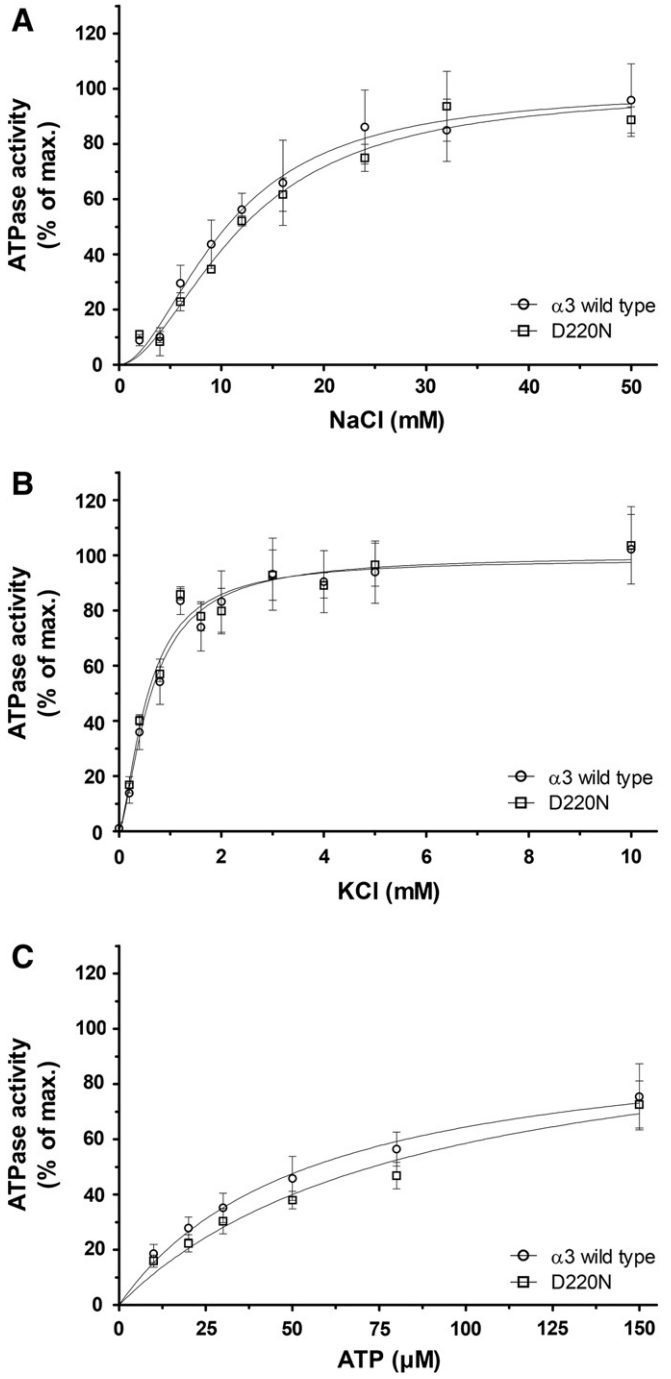

Fig. 4. Effect of Na^+, K^+ and ATP on the ATPase activity of wild type and mutant Na^+, K^+-ATPase. Enzymes were incubated at 37 °C in the presence of 1.3 mM $MgCl_2$, 0.1 mM EGTA, 2.0 mM Tris-N_3, 50 mM Tris–acetic acid (pH 7.0), 50 mM or varying concentrations of NaCl (A), 5.0 mM or varying concentrations of KCl (B), and 100 μM or varying concentrations of ATP (C) for 30 min. Values are presented as mock corrected mean ± SEM with N ≥ 3.

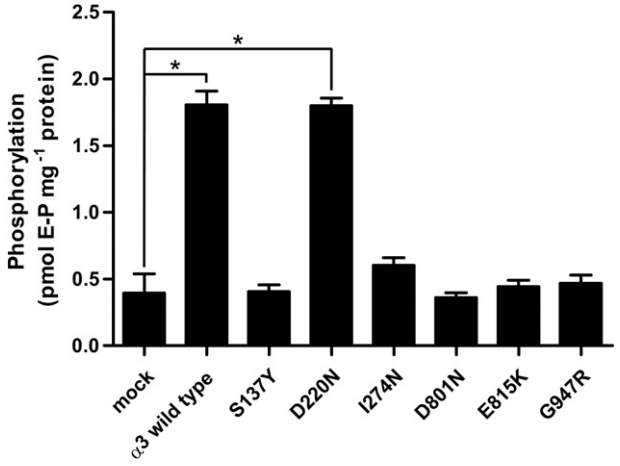

Fig. 5. ATP phosphorylation level of wild type and mutant Na^+,K^+-ATPase. Membranes expressing Na^+,K^+-ATPase were pre-incubated with 50 mM Tris–acetic acid (pH 7.0) 100 mM NaCl and 1.25 mM $MgCl_2$ at 0 °C for 30 min. Then, 0.1 μM radiolabeled ATP was added for 10 s before the reaction was stopped. Values are presented as mean ± SEM with $N \geq 3$. *$p < 0.05$ versus mock, ANOVA with Dunnett's post test.

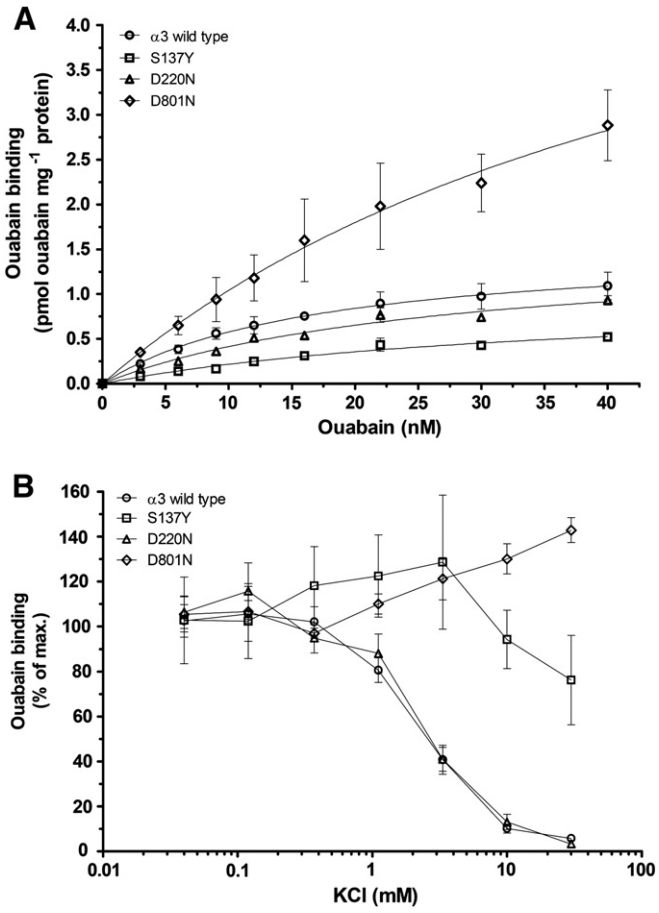

Fig. 6. (A) Ouabain-binding capacity of wild type and mutant Na^+,K^+-ATPase. Membranes were incubated at room temperature in the presence of 50 mM histidine at pH 7.0, 10 mM $MgCl_2$, 5 mM H_3PO_4, 25 nM radiolabeled ouabain and different concentrations of non-radiolabeled ouabain. Values are presented as mean ± SEM with $N \geq 3$. Three mutants (I274N, E815K and G947R) did not bind ouabain and are not shown. (B) The effect of K^+ on ouabain binding. Membranes were incubated at room temperature in the presence of 50 mM histidine at pH 7.0, 10 mM $MgCl_2$, 5.0 mM H_3PO_4, 25 nM radiolabeled ouabain and increasing concentrations of KCl for 2 h. Values are presented as mean ± SEM with $N \geq 3$, corrected for values obtained in the absence of KCl.

3.6. K^+/ouabain antagonism is absent in S137Y and D801N

As described above, three mutants (S137Y, D220N and D801N) were able to bind ouabain (Fig. 6A), whereas only one of them (D220N) showed ATPase activity (Fig. 3). In order to determine whether the K^+-binding was affected, we studied the well-known antagonism between K^+ and ouabain (Fig. 1A). We measured the relative ouabain binding at increasing concentrations of KCl in the presence of 25 nM ouabain: a decrease in ouabain binding was seen for wild type and mutant D220N upon increasing KCl concentrations (Fig. 6B). The inhibitory effect of KCl on ouabain binding was not observed for S137Y and D801N, indicating that K^+ is not able to bind to these mutants.

3.7. In silico analysis of mutants

In silico analysis of three crystal structures representing α1β1 Na^+, K^+-ATPase in various conformations (E_1P–ADP, E_2P–ouabain, and $E_2 \cdot 2K^+ \cdot P_i$) resulted in the identification of various H-bond interactions involving the residues corresponding to Ser^{137} and Glu^{815}. In the E_2P–ouabain crystal structure, Ser^{137} was predicted to form a hydrogen bond with Gln^{85}, whereas Glu^{815} was involved in a network of H-bonds involving residues Asn^{761}, Lys^{928}, Asn^{937}, and Asn^{941} in multiple crystal structures. Finally, Gly^{947} was observed to have a limited space due to the close proximity of Val^{807} and Pro^{808} as observed for the E_2P–ouabain conformation.

4. Discussion

Alternating Hemiplegia of Childhood (AHC) is a rare, severe neurodevelopmental disorder caused by de novo mutations in the *ATP1A3* gene, coding for the α3-isoform of Na^+,K^+-ATPase. In this study we examined the functional consequences of six single mutations in *ATP1A3* associated with AHC. The amino acids affected in all six mutations are highly conserved in Na^+,K^+-ATPase, suggesting an important impact of the mutations on enzyme function [27]. Here, we discuss the relationship between functional activities of the mutants and the AHC phenotype. A summary of the experimental findings obtained for the mutants and wild type Na^+,K^+-ATPase is shown in Table 1.

4.1. D220N possesses biochemical characteristics similar to wild type enzyme

In general, AHC mutations are located near or inside one of the transmembrane domains. One exception to this rule appears to be D220N, located in the cytosolic loop between transmembrane domains 2 and 3 (Fig. 1B). We could not identify any statistically significant differences between D220N and the wild type enzyme. Protein expression, ATPase activity, apparent Na^+, K^+, and ATP affinities, phosphorylation, ouabain binding, as well as the ouabain/K^+ antagonism were all similar to those of wild type enzyme. These results imply that this mutation is possibly not pathogenic, although we have not investigated protein localization. Further studies are required to explain the severe phenotype reported for this mutation [8].

4.2. Catalytic activity

All six *ATP1A3* mutants were expressed at protein levels comparable to that of wild type enzyme. However, no significant ATPase activity or phosphorylation level was detected for S137Y, I274N, D801N, E815K and G947R. Moreover, I274N, E815K, and G947R could not bind ouabain, which indicates that these mutations result in a severely affected protein with a complete loss of function.

Whereas almost all AHC-linked mutations are de novo, I274N was reported in a family with several members suffering from a form of

Table 1
Summary of catalytic properties of wild type and mutant Na^+,K^+-ATPase. Data represent the mean ± SEM of three enzyme preparations corrected for background values.

	ATPase activity studies				Ouabain binding studies			Phosphorylation
	ATPase activity μmol P_i mg^{-1} h^{-1}	Na^+ $K_{0.5}$ mM	K^+ $K_{0.5}$ mM	ATP $K_{0.5}$ μM	Max. binding pmol mg^{-1} protein	Ouabain K_d nM	K^+/ouabain antagonism IC_{50} (mM)	
Wild type	0.94 ± 0.11*	11 ± 1	0.62 ± 0.1	55 ± 19	1.55 ± 0.20*	17 ± 5	2.7 ± 1.1	1.42 ± 0.10*
S137Y	−0.12 ± 0.07		–	–	1.01 ± 0.17*	37 ± 10	»	0.07 ± 0.05
D220N	0.71 ± 0.05*	12 ± 1	0.56 ± 0.1	86 ± 27	1.53 ± 0.16*	27 ± 5	2.9 ± 1.2	1.43 ± 0.06*
I274N	0.07 ± 0.03	–	–	–	Not converged	–	–	0.21 ± 0.06
D801N	−0.03 ± 0.06	–	–	–	6.62 ± 2.58*	54 ± 31	»	−0.03 ± 0.04
E815K	−0.07 ± 0.02	–	–	–	Not converged	–	–	0.05 ± 0.08
G947R	−0.09 ± 0.06	–	–	–	−0.02 ± 0.01	–	–	0.07 ± 0.11

– = not determined, * = $p < 0.05$ vs mock, » = exceeding tested range.

alternating hemiplegia [8]. Kirshenbaum et al. modeled the structure of Na^+,K^+-ATPase with I274N, which showed a loss of interaction between Glu^{776} with its interacting K^+ atom and also a disturbance of the side-chain interaction between Thr^{272} and Ile^{274} [12]. These changes might seriously impact protein functionality, thereby explaining the lack of ATPase activity.

The absence of ATPase activity in mutant E815K was reported previously in a study using COS-7 cells [8]. In three crystal structures, representing the E_1P–ADP, E_2P–ouabain and $E_2 \cdot 2K^+ \cdot P_i$ conformations (4HQJ [24], 4HYT [25] and 2ZXE [26], respectively), we could identify an extensive interaction network between the side chains of Glu^{815} with Asn^{761}, Lys^{928}, Asn^{937} and Asn^{941}, which is possibly affected by replacement of the negatively charged glutamic acid by a positively charged lysine.

Mutant G947R is located in transmembrane domain 9. Being located in an α-helix, a change from glycine to arginine might strongly disturb the helix structure. Based on a crystal structure representing the E_2P–ouabain conformation (4HYT [25]), we found that the side chain of arginine at this position has limited space, as residues Val^{807} and Pro^{808} (in transmembrane domain 6) are located near Gly^{947}. Also, Gly^{947} is located close to Glu^{951}, important in regulating the C-terminal ion pathway [28]. In addition, a recently published crystal structure of the Na^+-bound state suggested that G947R affects the IIIa ion binding site of Na^+,K^+-ATPase, which is important for the release of Na^+ ions following transition from the E_1P–ADP state to the E_2P state [24].

4.3. Ouabain and K^+ binding

S137Y and D801N failed to show ATPase activity, whereas significant ouabain binding was present. We conclude that these two mutations result in a correctly folded protein, capable of binding ouabain, yet with an impaired reaction cycle. It appeared that they can transit into the ouabain binding E_2P conformation, indicating that the conformation that is affected involves the Na^+ binding E_1 state. The absence of phosphorylated protein also points in this direction, as ATP phosphorylation occurs via the E_1 state of the enzyme.

The ouabain binding capacity of these mutants allows us to evaluate the K^+ binding capacity. It is known that ouabain and K^+ act as antagonists, and a change in K^+ affinity should therefore be reflected by a shift in the K^+/ouabain competition curve. Although the amount of ouabain bound enzyme was decreased for wild type and D220N, we could not observe this phenomenon for S137Y and D801N. This indicates that the latter mutations decrease the affinity for K^+, which together with the absence of phosphorylation suggest that S137Y and D801N affect cation binding in general.

Whereas this study reports on the biochemical effects of the S137Y mutation, low ATPase activity for S137F was reported before in COS-7 cells [8]. Ser^{137} is located within the second transmembrane domain where it forms an H-bond with Gln^{85} as based on our in silico analysis of the recently published E_2P–ouabain structure [25]. Gln^{85} is located just before the characteristic TM1 kink, important in the N-terminal ion pathway of the enzyme [29], through which the cations pass. Replacing the serine with a tyrosine might have a strong impact on the interaction between serine and glutamine, due to the bulky aromatic ring in the side chain of tyrosine.

Mutant D801N belongs to the most frequent mutations in AHC cases [8,9]. This mutation has been reported to reduce ATPase activity in COS-7 cells [8], in accordance with our results. In addition, we have previously shown a lack of phosphorylation for the corresponding residue (Asp^{804}) in rat α1 Na^+,K^+-ATPase [30]. Contrary to our results, Pedersen et al. described the phosphorylation of mutant D804N after Na^+ stimulation in yeast cells [31]. Structural modeling of the D801N mutation predicted a direct effect on binding of potassium ions [8,12], reflecting the highly important role of Asp^{801} in coordination of ion binding sites I and II in K^+-occlusion [32] and Na^+-coordination [24,33], and also binding of a Mg^{2+} ion in site II in the high resolution ouabain bound structure [25]. We speculate that replacing aspartic acid with asparagine at this position increases the preference of the enzyme for the E_2P-DLC conformation by decreasing the preference for the E_2P conformation. For rat Na^+,K^+-ATPase α1 it was already known that Asp^{804} (corresponding to Asp^{801} in human) plays a major role in the cation binding pocket [31,34].

4.4. Mechanism of disease

Unfortunately, the exact mechanism of disease for *ATP1A3* mutations remains to be understood. It is known that the alpha 3 subunit of Na^+,K^+-ATPase is found mainly in the central and peripheral nervous system, and therefore it is not surprising that these mutations have a neurological effect. The first study to look at the functional consequences of AHC at the cellular level was published recently [35], reporting a structural and functional granule defect in platelets and fibroblasts of AHC patients. Furthermore, increased cathepsin B-dependent apoptosis in fibroblasts was observed, linking lysosomal defects to decreased ATPase activity.

It is highly challenging to correlate changes in biochemical characteristics to the frequency and duration of attacks in patients suffering from AHC. However, due to the high frequency of D801N and E815K, responsible for most AHC cases, it was possible to show that E815K causes a more severe phenotype than D801N [10]. Although both enzymes are catalytically inactive, we found that D801N is able to bind ouabain, whereas E815K is not. Possibly, the lack of ouabain binding might link E815K to its severe phenotype. Previous studies have shown that ouabain and other digitalis-like compounds are produced endogenously, both in adrenal cells as well as in the hypothalamus [36]. The role of Na^+,K^+-ATPase as a signal transducer might provide an explanation for the less severe phenotype observed for mutation D801N compared with mutation E815K. A possible role of endogenous ouabain in AHC should be the subject of future studies.

4.5. Conclusion

Our study is the first to show in detail the biochemical properties of six AHC causing mutations, and reveals that mutations in *ATP1A3* affect the functionality of Na^+,K^+-ATPase, which might explain why they are associated with AHC. However, no differences in protein function were observed for mutant D220N compared to wild type Na^+,K^+-ATPase. Mutants I274N, E815K, and G947R did not result in functional protein as reflected by a complete loss of ouabain binding and ATPase activity, rendering them unsuitable for further studies. Mutants S137Y and D801N could bind ouabain, but showed no ATPase activity, no phosphorylation, and an impaired K^+ binding. The presence of ouabain binding might provide an explanation for the less severe phenotype observed for D801N as compared to E815K.

Disclosure statement

The authors declare that there are no conflicts of interest.

Acknowledgements

Financial support for this study was provided by a personal VIDI-grant (700.58.427) from the Netherlands Organisation for Scientific Research to J.B.K. There was no involvement of the funding source with any part of the research performed or decision to submit this article.

References

[1] S. Verret, J.C. Steele, Alternating hemiplegia in childhood: a report of eight patients with complicated migraine beginning in infancy, Pediatrics 47 (1971) 675–680.
[2] B.G. Neville, M. Ninan, The treatment and management of alternating hemiplegia of childhood, Dev. Med. Child Neurol. 49 (2007) 777–780.
[3] M. Bourgeois, J. Aicardi, F. Goutieres, Alternating hemiplegia of childhood, J. Pediatr. 122 (1993) 673–679.
[4] M.A. Mikati, U. Kramer, M.L. Zupanc, R.J. Shanahan, Alternating hemiplegia of childhood: clinical manifestations and long-term outcome, Pediatr. Neurol. 23 (2000) 134–141.
[5] M.T. Sweney, K. Silver, M. Gerard-Blanluet, J.M. Pedespan, F. Renault, A. Arzimanoglou, et al., Alternating hemiplegia of childhood: early characteristics and evolution of a neurodevelopmental syndrome, Pediatrics 123 (2009) e534–e541.
[6] P. Casaer, M. Azou, Flunarizine in alternating hemiplegia in childhood, Lancet 2 (1984) 579.
[7] K. Silver, F. Andermann, Alternating hemiplegia of childhood: a study of 10 patients and results of flunarizine treatment, Neurology 43 (1993) 36–41.
[8] E.L. Heinzen, K.J. Swoboda, Y. Hitomi, F. Gurrieri, S. Nicole, B. de Vries, et al., De novo mutations in ATP1A3 cause alternating hemiplegia of childhood, Nat. Genet. 44 (2012) 1030–1034.
[9] H. Rosewich, H. Thiele, A. Ohlenbusch, U. Maschke, J. Altmuller, P. Frommolt, et al., Heterozygous de-novo mutations in ATP1A3 in patients with alternating hemiplegia of childhood: a whole-exome sequencing gene-identification study, Lancet Neurol. 11 (2012) 764–773.
[10] M. Sasaki, A. Ishii, Y. Saito, N. Morisada, K. Iijima, S. Takada, et al., Genotype–phenotype correlations in alternating hemiplegia of childhood, Neurology 82 (2014) 482–490.
[11] P. de Carvalho Aguiar, K.J. Sweadner, J.T. Penniston, J. Zaremba, L. Liu, M. Caton, et al., Mutations in the Na^+/K^+-ATPase alpha3 gene ATP1A3 are associated with rapid-onset dystonia Parkinsonism, Neuron 43 (2004) 169–175.
[12] G.S. Kirshenbaum, N. Dawson, J.G. Mullins, T.H. Johnston, M.J. Drinkhill, I.J. Edwards, et al., Alternating hemiplegia of childhood-related neural and behavioural phenotypes in Na^+,K^+-ATPase alpha3 missense mutant mice, PLoS ONE 8 (2013) e60141.
[13] A. Roubergue, E. Roze, S. Vuillaumier-Barrot, M.J. Fontenille, A. Meneret, M. Vidailhet, et al., The multiple faces of the ATP1A3-related dystonic movement disorder, Mov. Disord. 28 (2013) 1457–1459.
[14] M. Sasaki, A. Ishii, Y. Saito, S. Hirose, Intermediate form between alternating hemiplegia of childhood and rapid-onset dystonia–parkinsonism, Mov. Disord. 29 (2014) 153–154.
[15] E.E. Benarroch, Na^+,K^+-ATPase: functions in the nervous system and involvement in neurologic disease, Neurology 76 (2011) 287–293.
[16] J.H. Kaplan, Biochemistry of Na,K-ATPase, Ann. Rev. Biochem. 71 (2002) 511–535.
[17] J.P. Morth, B.P. Pedersen, M.J. Buch-Pedersen, J.P. Andersen, B. Vilsen, M.G. Palmgren, P. Nissen, A structural overview of the plasma membrane Na^+, K^+-ATPase and H^+-ATPase ion pumps, Nat. Rev. Mol. Cell Biol. 12 (2011) 60–70.
[18] V.A. Luckow, S.C. Lee, G.F. Barry, P.O. Olins, Efficient generation of infectious recombinant baculoviruses by site-specific transposon-mediated insertion of foreign genes into a baculovirus genome propagated in *Escherichia coli*, J. Virol. 67 (1993) 4566–4579.
[19] A.A. El-Sheikh, J.J. van den Heuvel, E. Krieger, F.G. Russel, J.B. Koenderink, Functional role of arginine 375 in transmembrane helix 6 of multidrug resistance protein 4 (MRP4/ABCC4), Mol. Pharmacol. 74 (2008) 964–971.
[20] H.G. Swarts, J.B. Koenderink, P.H. Willems, J.J. De Pont, The non-gastric H, K-ATPase is oligomycin-sensitive and can function as an H^+, NH4(+)-ATPase, J. Biol. Chem. 280 (2005) 33115–33122.
[21] J.B. Koenderink, S. Geibel, E. Grabsch, J.J. De Pont, E. Bamberg, T. Friedrich, Electrophysiological analysis of the mutated Na,K-ATPase cation binding pocket, J. Biol. Chem. 278 (2003) 51213–51222.
[22] J.B. Koenderink, H.G. Swarts, H.P. Hermsen, J.J. De Pont, The beta-subunits of Na^+, K^+-ATPase and gastric H^+,K^+-ATPase have a high preference for their own alpha-subunit and affect the K^+ affinity of these enzymes, J. Biol. Chem. 274 (1999) 11604–11610.
[23] L.Y. Qiu, J.B. Koenderink, H.G. Swarts, P.H. Willems, J.J. De Pont, Phe783, Thr797, and Asp804 in transmembrane hairpin M5–M6 of Na^+,K^+-ATPase play a key role in ouabain binding, J. Biol. Chem. 278 (2003) 47240–47244.
[24] M. Nyblom, H. Poulsen, P. Gourdon, L. Reinhard, M. Andersson, E. Lindahl, N. Fedosova, P. Nissen, Crystal structure of Na^+,K^+-ATPase in the Na^+-bound state, Science 342 (2013) 123–127.
[25] M. Laursen, L. Yatime, P. Nissen, N.U. Fedosova, Crystal structure of the high-affinity Na^+,K^+-ATPase–ouabain complex with Mg^{2+} bound in the cation binding site, Proc. Natl. Acad. Sci. U. S. A. 110 (2013) 10958–10963.
[26] T. Shinoda, H. Ogawa, F. Cornelius, C. Toyoshima, Crystal structure of the sodium–potassium pump at 2.4 A resolution, Nature 459 (2009) 446–450.
[27] A. Ishii, Y. Saito, J. Mitsui, H. Ishiura, J. Yoshimura, H. Arai, et al., Identification of ATP1A3 mutations by exome sequencing as the cause of alternating hemiplegia of childhood in Japanese patients, PLoS ONE 8 (2013) e56120.
[28] H. Poulsen, H. Khandelia, J.P. Morth, M. Bublitz, O.G. Mouritsen, J. Egebjerg, P. Nissen, Neurological disease mutations compromise a C-terminal ion pathway in the Na(+)/K(+)-ATPase, Nature 467 (2010) 99–102.
[29] A. Takeuchi, N. Reyes, P. Artigas, D.C. Gadsby, The ion pathway through the opened Na(+), K(+)-ATPase pump, Nature 456 (2008) 413–416.
[30] J.B. Koenderink, H.G. Swarts, H.P. Hermsen, P.H. Willems, J.J. De Pont, Mutation of aspartate 804 of Na(+),K(+)-ATPase modifies the cation binding pocket and thereby generates a high Na(+)-ATPase activity, Biochemistry 39 (2000) 9959–9966.
[31] P.A. Pedersen, J.H. Rasmussen, J.M. Nielsen, P.L. Jorgensen, Identification of Asp804 and Asp808 as Na^+ and K^+ coordinating residues in alpha-subunit of renal Na,K-ATPase, FEBS Lett. 400 (1997) 206–210.
[32] J.P. Morth, B.P. Pedersen, M.S. Toustrup-Jensen, T.L. Sorensen, J. Petersen, J.P. Andersen, B. Vilsen, P. Nissen, Crystal structure of the sodium–potassium pump, Nature 450 (2007) 1043–1049.
[33] R. Kanai, H. Ogawa, B. Vilsen, F. Cornelius, C. Toyoshima, Crystal structure of a Na-bound Na,K-ATPase preceding the E_1P state, Nature 502 (2013) 201–206.
[34] T.A. Kuntzweiler, J.M. Arguello, J.B. Lingrel, Asp804 and Asp808 in the transmembrane domain of the Na,K-ATPase alpha subunit are cation coordinating residues, J. Biol. Chem. 271 (1996) 29682–29687.
[35] M. Di Michele, C. Goubau, E. Waelkens, C. Thys, R. De Vos, L. Overbergh, et al., Functional studies and proteomics in platelets and fibroblasts reveal a lysosomal defect with increased cathepsin-dependent apoptosis in ATP1A3 defective alternating hemiplegia of childhood, J. Proteomics 86 (2013) 53–69.
[36] A.Y. Bagrov, J.I. Shapiro, O.V. Fedorova, Endogenous cardiotonic steroids: physiology, pharmacology, and novel therapeutic targets, Pharmacol. Rev. 61 (2009) 9–38.